nature medicine

Article

https://doi.org/10.1038/s41591-026-04287-9

An international mega-analysis of psychedelic drug effects on brain circuit function

Received: 25 March 2025

Accepted: 12 February 2026

Published online: 6 April 2026

Check for updates

A list of authors and their affiliations appears at the end of the paper

Psychedelic drugs are re-emerging as promising scientific and clinical tools. However, despite a rapidly expanding literature on their therapeutic value, the neural mechanisms underlying psychedelic effects remain unclear. Resting-state functional magnetic resonance imaging studies of acute psychedelic effects, conducted independently by several research groups, have so far yielded fragmented and sometimes inconsistent findings. Here, to help facilitate greater convergence, we conducted a 'mega-analysis' integrating 11 independent resting-state functional magnetic resonance imaging datasets across five psychedelic drugs (psilocybin, lysergic acid diethylamide, mescaline, *N*,*N*-dimethyltryptamine and ayahuasca) from research groups spanning three continents and five countries. By applying a uniform preprocessing pipeline and a Bayesian hierarchical modeling framework, we discovered several common features in the induced alterations to brain function across drugs and sites. Most prominently, we identified a core signature of increased functional connectivity between transmodal (default, frontoparietal and limbic) and unimodal networks (visual and somatomotor), with subnetwork specificity. Furthermore, key subcortical regions (thalamus, caudate and putamen) and the cerebellum exhibited altered coupling with sensorimotor networks. In contrast to several single-site reports, Bayesian modeling revealed weak-to-moderate and selective reductions in within-network functional connectivity, with substantial variability across drugs and networks. Together, these findings extend past work by demonstrating that psychedelics reconfigure large-scale cortical organization while selectively engaging subcortical circuitry. This study provides the most comprehensive synthesis of psychedelic brain action to date, helping resolve inconsistencies and offering a probabilistic map of how psychedelics alter large-scale brain organization. We hereby provide a cornerstone to benchmark and shepherd future psychedelic neuroimaging research.

e-mail: manesh.girn@ucsf.edu; danilo.bzdok@mcgill.ca

After a half-a-century-long 'psychedelic research winter', psychedelic drugs have resurfaced as drivers of scientific insight and clinical innovation in mental health[1–3]. Characterized by their ability to induce wide-ranging changes to conscious experience, the so-called 'classic psychedelics,' which exert their primary effects through the shared mechanism of 5-HT2A receptor agonism, include psilocybin (the active compound in magic mushrooms), lysergic acid diethylamide (LSD), mescaline (the psychoactive alkaloid in certain cacti), *N*,*N*-dimethyltryptamine (DMT; found in many plant species and is the central ingredient of the psychedelic brew ayahuasca). These compounds have demonstrated strong therapeutic potential, with a combined total of over a dozen randomized, placebo-controlled clinical trials reporting efficacy in treating depression, end-of-life distress, generalized anxiety disorder, tobacco addiction and alcoholism[4,5]. Reflecting this rapid expansion of clinical interest, a current search for 'psychedelic therapy' on clinicaltrials.gov returns more than 400 active trials exploring these compounds as a potential treatment for psychiatric and neurological conditions. Ongoing trials span all four of the classic psychedelic classes which, despite the presence of pharmacological differences between them, are assumed implicitly to overlap in key mechanisms.

The growing promise of psychedelic-assisted therapy necessitates a deeper understanding of the neurobiological mechanisms underlying their effects, including the possibility of mechanistic overlap across distinct drug agents. Psychedelic neuroscience research has accelerated rapidly over the past decade, spanning from cellular-molecular investigations of neuronal morphology and plasticity[6,7] to investigations of large-scale functional networks in humans[8–10]. The latter investigations have relied primarily on (task-free) resting-state functional magnetic resonance imaging (rsfMRI)—a method measuring the spontaneous coordinated activity among brain regions. This approach has begun to shed light on the acute changes in neural activity and connectivity induced by psychedelic compounds and their relation to psychological effects. In addition to providing important mechanistic data to help inform regulatory decisions, progress in this area is promising for the development of precision medicine approaches for psychedelic therapy, including personalized treatment approaches and more reliable early-stage prognostics[11]. Progress also has potential to shed light on brain circuits relevant to mental health, as well as the neurobiological and psychological sequelae of brain circuit perturbation, which can help propel drug-based and neuromodulatory therapeutic innovation.

Despite compounding research interest, psychedelic rsfMRI studies in humans have so far been scattered into isolated efforts from separate research laboratories. These independent efforts have examined the changes in functional connectivity (FC; the covariation in two or more brain regions over time) induced by all of the classic psychedelics. Findings from this work suggest that psychedelics decrease FC within and increase FC between most large-scale cortical networks—a finding first observed by Roseman and colleagues[12] with psilocybin, and which has since been reported for additional drugs and datasets[9,12–18]. However, the specific network-level changes underlying these broad connectivity shifts have shown considerable heterogeneity across studies[9,19]. For example, a direct comparison of three existing datasets (two LSD, one psilocybin) failed to identify a single between-network FC increase consistently observed across all datasets[19]. Another notable inconsistency arises from 'global FC' analyses, which compute the mean whole-brain FC of individual regions to assess their overall integration with the rest of the brain. Strikingly, two independent research groups applying this approach to psychedelic neuroimaging data reported topographically opposite effect: one group found increased global FC in transmodal cortex and decreases in unimodal cortex across psilocybin, DMT and LSD datasets[14,20,21]), whereas the other reported a nearly inverse pattern for both LSD and psilocybin[22,23]. Accordingly, it is difficult to extract consistently confirmable conclusions from the current literature. This ambiguity probably stems, at least in part, from the methodological and analytical variability ('researcher's degrees of freedom') of this nascent and now rapidly evolving field[24–26], combined with practical challenges that have led to smaller sample sizes. Greater collaborative coordination across research groups is imperative for this field to move beyond this state of affairs. Such a joint effort may help convergence on a common understanding of psychedelic large-scale brain action.

To overcome several important limitations and help shape a more unified understanding of brain network reconfiguration under psychedelic drug influence, we conducted a mega-analysis that integrates intrinsic functional coupling data (rsfMRI) across several drugs, studies and research groups. We united the existing efforts in the psychedelic research community: spanning five countries, three continents and 11 distinct psychedelic neuroimaging datasets (n = 273, >550 connectomes). This mega-analysis brings together rsfMRI investigation of all four classic psychedelics—psilocybin, LSD, DMT (including ayahuasca, a DMT-containing brew with β-carbolines that enable its oral activity) and mescaline—under a uniform preprocessing and analysis pipeline. Collaborative coordination such as this is critical to converge on a common understanding of psychedelic large-scale brain action and counteract further fragmentation of this nascent literature. The present study seeks to lay down foundational bricks of evidence by playing this essential coordinative role.

To take concrete steps forward, we aimed to characterize how brain circuits are impacted by acute psychedelic drug action. We first sought to qualitatively delineate the consensus large-scale effects of psychedelics on functional brain organization, as revealed by the presently examined drug agents and data sources. We then built upon this with a bespoke Bayesian hierarchical modeling framework that affords a full probabilistic quantification of drug-induced effects across the examined drugs, explicitly taking into account study- and drug-specific variability. Unlike traditional null hypothesis testing, which relies on binary statistical thresholds, our Bayesian approach estimates full posterior distributions for each effect, enabling a principled quantification of uncertainty and a more nuanced understanding of the observed changes. This framework shifts the inferential question from "Does this effect exist?" to "How certain are we that this effect exists?" By providing results by means of both qualitative and Bayesian probabilistic approaches, our study offers a comprehensive synthesis of how classic psychedelics affect brain circuit function. Our primary aim was to identify the features of psychedelic brain action that reliably present across drugs and preprocessing pipelines, while also mapping drug-specific variability across large-scale circuits. By bridging methodological inconsistencies and consolidating findings across a series of studies, our confederated effort represents a critical step toward establishing a reproducible, data-driven framework for acute psychedelic neuroimaging.

Results

By carrying out a systematic mega-analysis pooled across 11 independent rsfMRI datasets, we were able to delineate the acute effects of psychedelics on human brain function. Results, encompassing 267 unique participants and more than 500 individual brain scanning sessions, painted a sharp picture of drug-mediated alterations in FC across brain regions and networks. For the sake of completeness and transparency, we present results for the aCompCor denoising pipeline with and without global signal regression (GSR). Results with the independent component analysis (ICA) with automatic removal of motion artifacts (ICA-AROMA) pipeline (with and without GSR) are presented in the Supplementary GitHub repository at https://github.com/banilo/BOLD_psychedelics_consortium.

Qualitative assessment of mean effects across all drugs and studies

To characterize the overall nature of psychedelic-induced changes in FC in a synoptic exploration, we first examined mean drug–placebo

https://doi.org/10.1038/s41591-026-04287-9

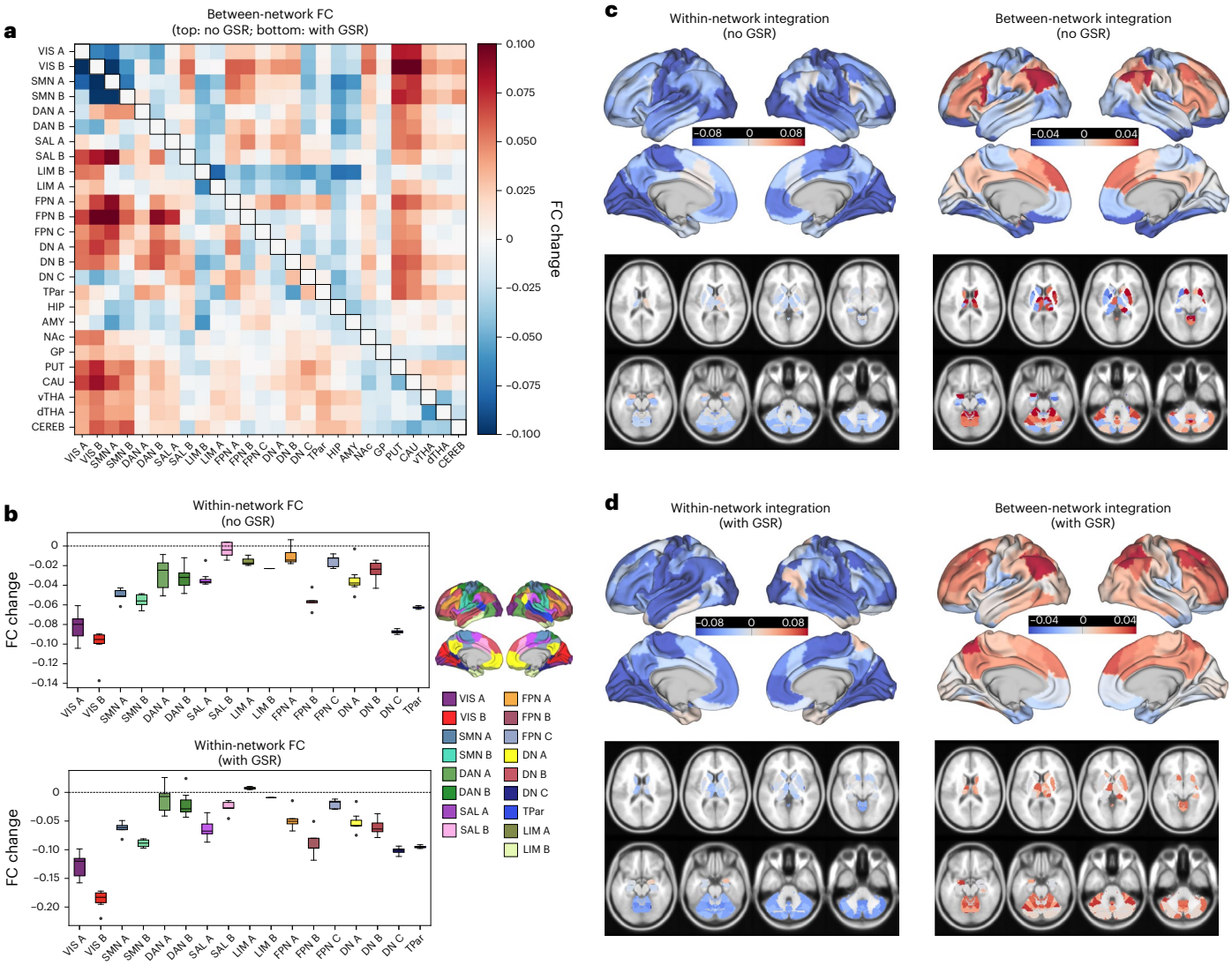

Fig. 1 | Changes in large-scale network functional coupling induced by psychedelic drugs, averaged across 4 drugs and 11 datasets. a, Mean drug–placebo difference in drug-induced between-network FC across all drugs and datasets, averaged for each cortical network (Schaefer–Yeo 100 parcel, 17-network) and subcortical and cerebellar region[51,52]. Upper right triangle: results without GSR; lower left triangle: results with GSR. Red and blue indicate drug-mediated increases and decreases in between-network FC, respectively. **b**, Mean drug–placebo difference in within-network FC for each cortical network (based on $n = 342$ participants). Boxplot values pertain to the mean within-network FC of each network's constituent regions. Data are presented as mean (mid-box line), 25th and 75th percentile (lower and upper box bound) and outliers (1.5× interquartile range as whiskers). **c**,**d**, Mean drug–placebo difference in the mean FC of each parcel with all parcels within its Yeo–Schaefer network ('Within-network integration') and the mean FC of each parcel with all parcels outside of its network ('Between-network integration'). Red and blue indicate higher and lower FC change, respectively. Kernel density plot display the distribution of within- (blue) and between- (green) network FC changes. Zero is marked with a vertical black line. Results are shown without GSR (**c**) and with GSR (**d**). Apparent group-level trends may not correspond to high-confidence Bayesian effects (reported in 'Bayesian posterior inference' below), which reflect both effect size and consistency across subjects and datasets.

differences across the 11 eligible datasets. Figure 1 presents these effects, averaged across cortical networks, subcortical regions and cerebellar regions. Region-wise drug-induced changes in cortical FC are shown in Supplementary Fig. 1. Note that these results are meant to offer a descriptive account of the observed mean differences and are before any formal modeling.

Between-network FC changes. Figure 1a displays the mean drug-induced changes in between-network FC, averaged across cortical networks and key subcortical regions. Both with and without GSR (lower and upper triangle, respectively; Fig. 1a), increases in between-network FC were strongest between transmodal association networks, such as the default network (DN) (DN_A) and frontoparietal network (FPN) (FPN_A and FPN_B) and unimodal/heteromodal sensory networks, such as visual (VIS) networks (VIS_A and VIS_B), somatomotor (SMN) networks (SMN_A and SMN_B) and dorsal attention networks (DAN) (DAN_A and DAN_B). Prominent increases in FC with sensorimotor networks were also evident for subcortical regions—most notably, the putamen (PUT) and caudate (CAU) without GSR, and PUT, CAU, the thalamus (ventral thalamic nuclei (vTHA) and dorsal thalamic nuclei (dTHA)) and cerebellum (CEREB) with GSR. Furthermore, several reductions in FC in between-network emerged. With GSR, this was observed predominantly between VIS and SMN networks, with scattered decreases elsewhere. Without GSR, reductions in FC between sensory networks were also observed, as well as between limbic networks and association networks, and

between the amygdala (AMY) and hippocampus (HIP) and most cortical networks.

Within-network FC changes. Figure 1b displays within-network FC changes across cortical networks, with results separately shown for pipelines with (bottom) and without (top) GSR. For both pipelines, all networks showed a mean decrease in within-network FC, with the single exception of limbic (LIM) A (LIM_A) with GSR. The strongest reductions were observed in VIS (VIS_A and VIS_B), SMN (SMN_A and SMN_B) and DN_C networks. Subcortical results (Supplementary Fig. 3) revealed decreased integration within all regions (that is, across the subparcels that comprise each structure), both with and without GSR.

Parcel-wise within- and between-network integration. Figure 1c,d display the region-wise mapping of mean parcel-wise within-network (left) and between-network (right) integration for each denoising pipeline. Both with and without GSR, reductions in within-network FC were observed across the cortex and subcortex—with frontal, temporal and left-lateralized lateral parietal regions showing stronger reductions with GSR. With regard to between-network FC, with GSR, cortical and subcortical regions both showed increases in predominantly between-network FC. Strongest increases were observed in lateral parietal and frontal regions, as well as along the cingulate gyrus. Weak decreases were observed in medial temporal and orbitofrontal regions, as well as the temporal sulcus. Without GSR, increases in between-network FC were more circumscribed and observed predominantly in lateral parietal and frontal regions, as well as dorsomedial prefrontal cortex. In the subcortex, increases were predominantly in the CEREB as well as the mostly right-lateralized CAU and PUT. Prominent reductions in between-network FC were observed in medial temporal and orbitofrontal regions. Minimal hemisphere-specific effects in absolute global FC were observed, as shown for cortical networks in Supplementary Fig. 4 and for subcortical regions in Supplementary Fig. 5.

Qualitative assessment of drug-specific effects

Next we examined the drug-induced changes in mean FC within- and between-network for each drug separately, with and without GSR (Fig. 2). Region-wise drug-induced changes in cortical FC are shown in Supplementary Fig. 2.

Psilocybin and LSD. Psilocybin (six datasets; $n = 106$ total) and LSD (four datasets; $n = 119$ total) revealed FC changes highly similar to each other and to the all-drugs results. With and without GSR both compounds showed widespread increases in between-network FC, particularly among transmodal association networks (FPN_A and FPN_B, DN_A), as well as LIM_A and unimodal/heteromodal sensorimotor networks (VIS, SMN, DAN and salience (SAL)). Increased FC between subcortical regions and sensorimotor networks was also observed and was particularly prominent for LSD. Decreased FC between sensorimotor regions was also observed for both drugs. For LSD, GSR led to further decreases in between-network FC, involving LIM networks as well as temporoparietal network (TPar), HIP, AMY and nucleus accumbens (NAc).

***N*,*N*-dimethyltryptamine.** DMT (one dataset; $n = 16$) exhibited the largest drug response effect of the drugs and featured a pattern largely resembling an amplified version of the psilocybin, LSD and all-drugs average. Of note, frontoparietal (FPN_A, FPN_B, FPN_C) and DN (DN_A, DN_B) networks, as well as CAU, vTHA and dTHA, showed particularly pronounced increases in FC with unimodal/heteromodal sensorimotor networks (VIS, SMN, DAN, SAL). DMT also induced strong FC reductions within and between VIS (VIS_A and VIS_B), SMN (SMN_A and SMN_B) and DAN_A networks, as well as between globus pallidus (GP), PUT, CAU, vTHA, dTHA and CEREB. LIM networks showed strong reductions in FC with the rest of the brain after GSR.

Mescaline. Mescaline (one dataset; $n = 31$) exhibited a pattern that moderately resembled that of psilocybin, LSD, DMT and all drugs. Without GSR, we observed widespread increases in between-network FC, with the most prominent effects occurring between SAL_B, LIM_A, FPN_A, FPN networks (FPN_A, FPN_B, FPN_C), DN_A, DN_B and sensorimotor networks (VIS, SMN and DAN), broadly mirroring effects seen in psilocybin and LSD. Also, similar to psilocybin and LSD, strong increases between each of the NAc, GP and dTHA, and cortical regions were observed. With GSR, FC increases were predominantly attenuated, with pronounced changes persisting between sensorimotor and association networks, as well as involving PUT and CAU.

Ayahuasca. Ayahuasca (one dataset; $n = 9$) exhibited a relatively idiosyncratic pattern of FC changes. In contrast to the other examined drugs, results without GSR revealed reduced FC between most networks and did not reveal a pattern of increased FC between unimodal and transmodal networks. With GSR, prominent reductions in FC were observed between unimodal/heteromodal sensorimotor networks (VIS, SMN, DAN, SAL), as well as between LIM_A, DN_C, HIP and AMY and sensorimotor networks. Increases were scattered, with prominent decreases between several subcortical regions (PUT, CAU, vTHA, dTHA) and sensorimotor networks. Without GSR, prominent decreases were also observed involving LIM networks, SAL_B, FPN_C and other scattered network pairs.

Bayesian posterior inference

After qualitatively assessing the broad topography of psychedelic-induced changes in large-scale network connectivity, we next applied Bayesian hierarchical inference (Methods) to formally quantify the strength and uncertainty of these effects across drugs and studies[27,28]. Although some mean effects seemed prominent in average FC matrices, not all reached high-confidence levels in the Bayesian analyses. This reflects the model's sensitivity to intersubject variability and noise, highlighting only those effects with robust, consistent support across drugs and datasets. Unlike traditional frequentist approaches aiming at categorical yes/no answers on effects, our Bayesian framework allows for graded probabilistic inference by answering the question: 'How sure are we that these two brain regions/networks change in FC as a result of psychedelic drug effects?' We constructed Bayesian models for each network (intra-network FC) and network pair (between-network FC), deriving full posterior distributions for each drug's estimated effects. Robust cross-psychedelic effects are those that have distributions that (1) are distant from zero, (2) show relatively low dispersion and (3) show overlap/consistency in divergence from zero across drugs. We avoid strict thresholds as these would be, by necessity, arbitrary and in opposition to Bayesian thinking, and instead allow readers to make their own judgments on the basis of the posterior distributions provided. Bayesian posterior distributions for the most prominent

Fig. 2 | Drug-specific changes in inter-regional and inter-network functional coupling. Mean drug–placebo FC difference within and between each of the 17 cortical networks and subcortical regions for each drug separately. The 'All drugs' average is displayed for comparison. Cortical networks are based on the 17-network, 100 parcel Schaefer–Yeo parcellation[53]. Upper right triangles: results without GSR; lower left triangles: results with GSR. Subcortical regions based on ref. 51. CEREB based on Buckner ref. 52. Red and blue indicate drug-mediated increases and decreases in inter-regional FC, respectively; n = number of connectomes, following exclusion of those with high motion (Methods). Apparent group-level trends may not correspond to high-confidence Bayesian effects (reported in 'Bayesian posterior inference' below), which reflect both effect size and consistency across subjects and datasets.

https://doi.org/10.1038/s41591-026-04287-9

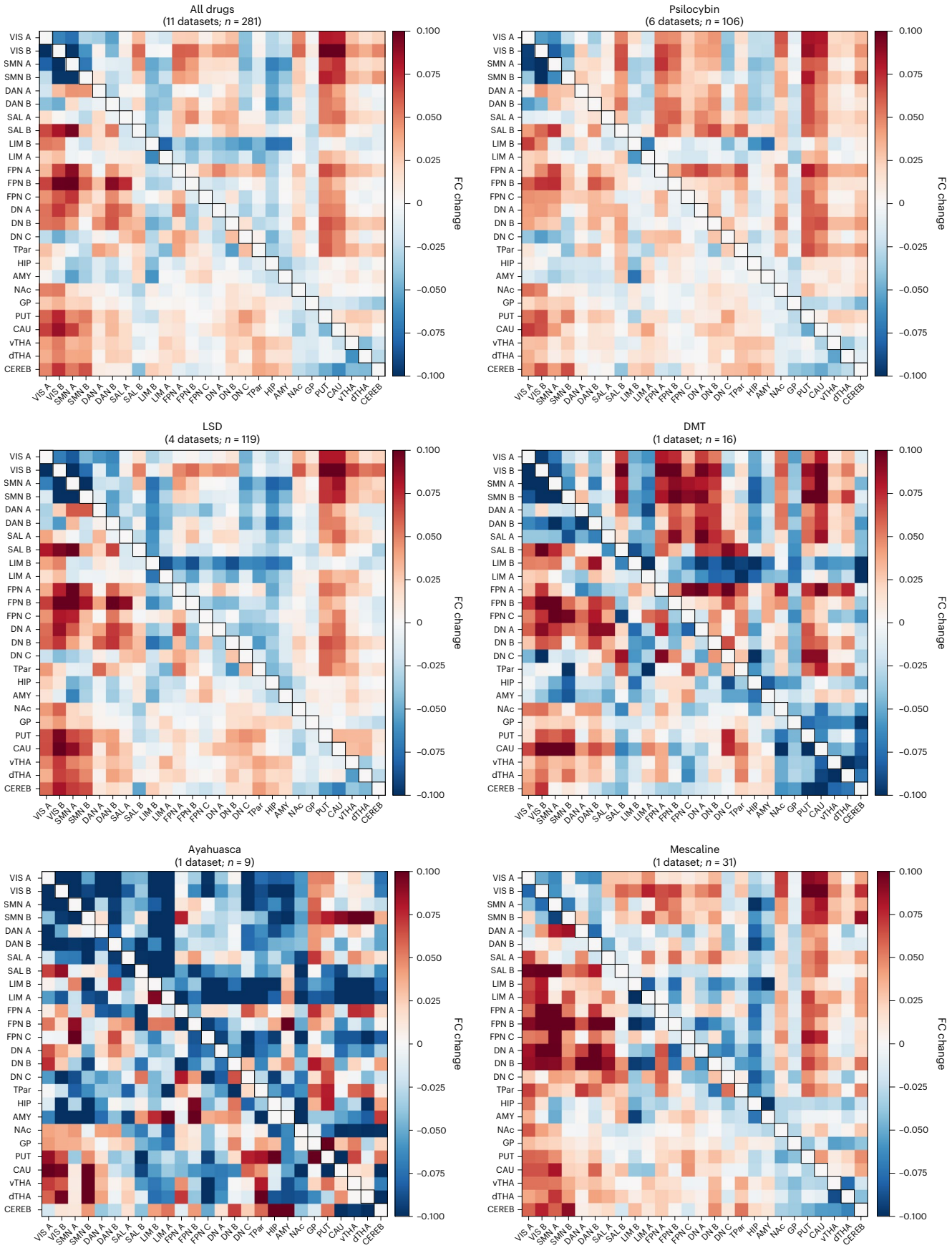

https://doi.org/10.1038/s41591-026-04287-9

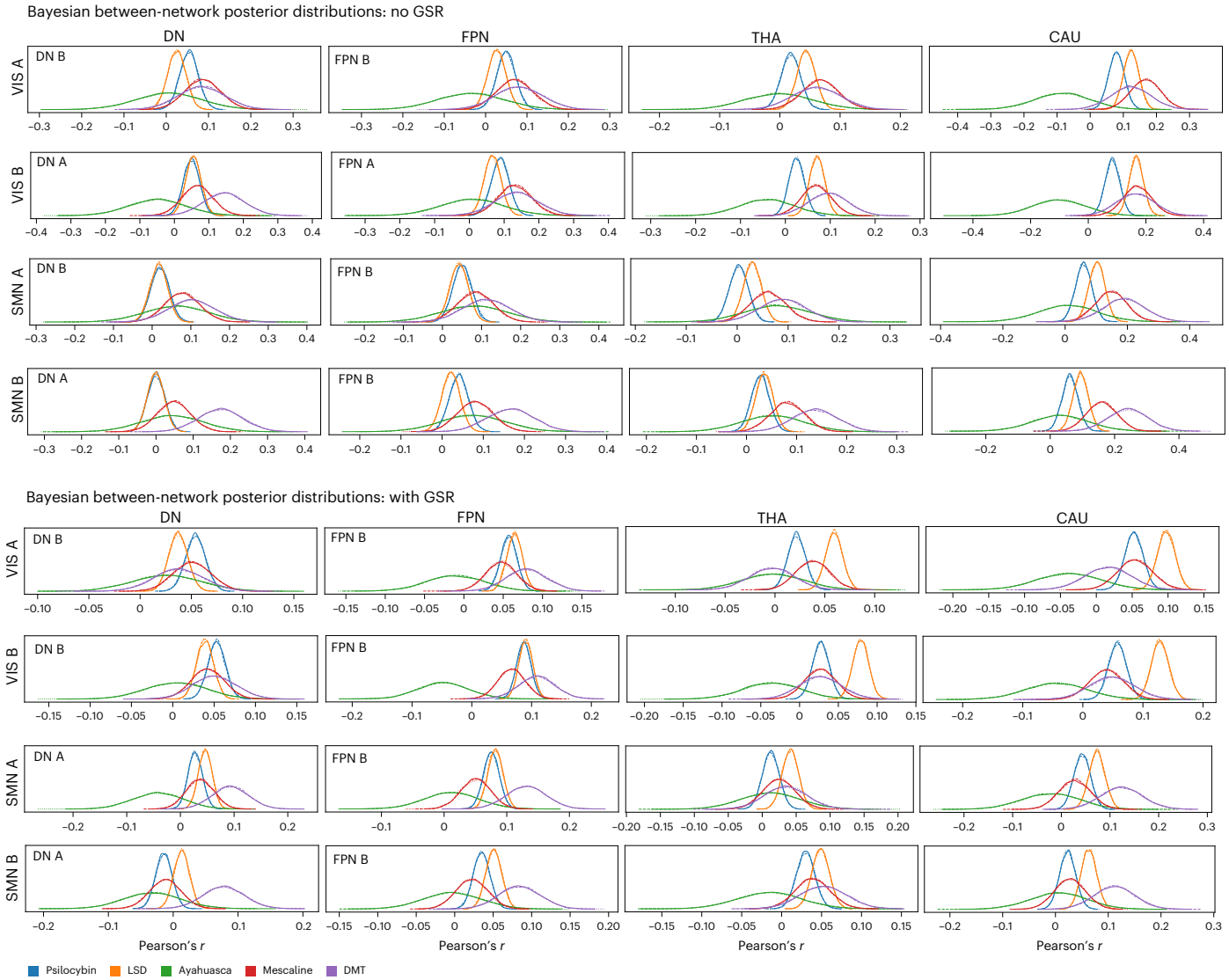

Fig. 3 | Bayesian posterior inference of between-network effects across drugs. Posterior distribution plots from Bayesian modeling for the largest nonzero effects in drug-mediated changes in between-network FC for each drug. These posterior distributions provide principled, probabilistically grounded estimates of both the uncertainty (as indicated by distribution width) and magnitude (as indicated by the peak location on the *x* axis) of drug-induced effects for each modeled drug class. The *x* axis represents change in Pearson's product–moment correlation coefficient (*r*) between conditions (drug–placebo) and the *y* axis represents Bayesian probability in unspecified units.

between-network FC changes (based on our noninferential descriptive analyses) are shown in Fig. 3 (additional results available in the Supplementary GitHub Repository at https://github.com/banilo/BOLD_psychedelics_consortium). Across network pairs, posterior inference revealed a consistent pattern of increased between-network coupling, with effect magnitudes and certainty varying by drug, network pair and preprocessing choice. Distributions were most commonly overlapping for LSD and psilocybin and, to a lesser extent, mescaline. Distributions for these three drugs also demonstrate the least dispersion, explained, probably at least partly, by larger sample sizes in these drug groups. Less dispersion or tighter posterior distributions increases confidence that similarities between LSD and psilocybin may be meaningful and reliable. Ayahuasca and DMT tended to exhibit the least certainty in effects, probably owing to the converse—namely, single studies and relatively small sample sizes.

Without GSR, the strongest and most consistently positive posterior shifts were observed for CAU coupling with unimodal networks, including CAU–VIS_A, CAU–VIS_B, CAU–SMN_A and CAU–SMN_B. Robust positive shifts were also evident for cross-network coupling between VIS and transmodal subnetworks, most prominently DN_A–VIS_B, DN_B–VIS_A, FPN_B–VIS_A and FPN_A–VIS_B, as well as for SMN–frontoparietal coupling, particularly FPN_B–SMN_A. In contrast, THA coupling showed posterior distributions that were consistently negatively skewed across all VIS and SMN subnetworks. With GSR, posterior distributions across these between-network pairings were generally shifted in a more positive direction, although the magnitude of this shift varied across drugs and network pairs.

Regarding within-network FC effects, Bayesian parameter distribution plots are shown in Fig. 4 for all 17 (sub)networks and the subcortical regions with the most prominent within-network effects (based on our noninferential descriptive analyses). Across networks, posterior distributions generally indicated weak-to-moderate reductions in within-network FC, with substantial variability in both effect magnitude and uncertainty across drugs and preprocessing pipelines. Although many distributions overlapped with zero, several networks exhibited consistent posterior shifts toward decreased within-network FC. Drug response effects were most reliable for psilocybin and LSD, which showed relatively narrow posterior distributions and consistent

https://doi.org/10.1038/s41591-026-04287-9

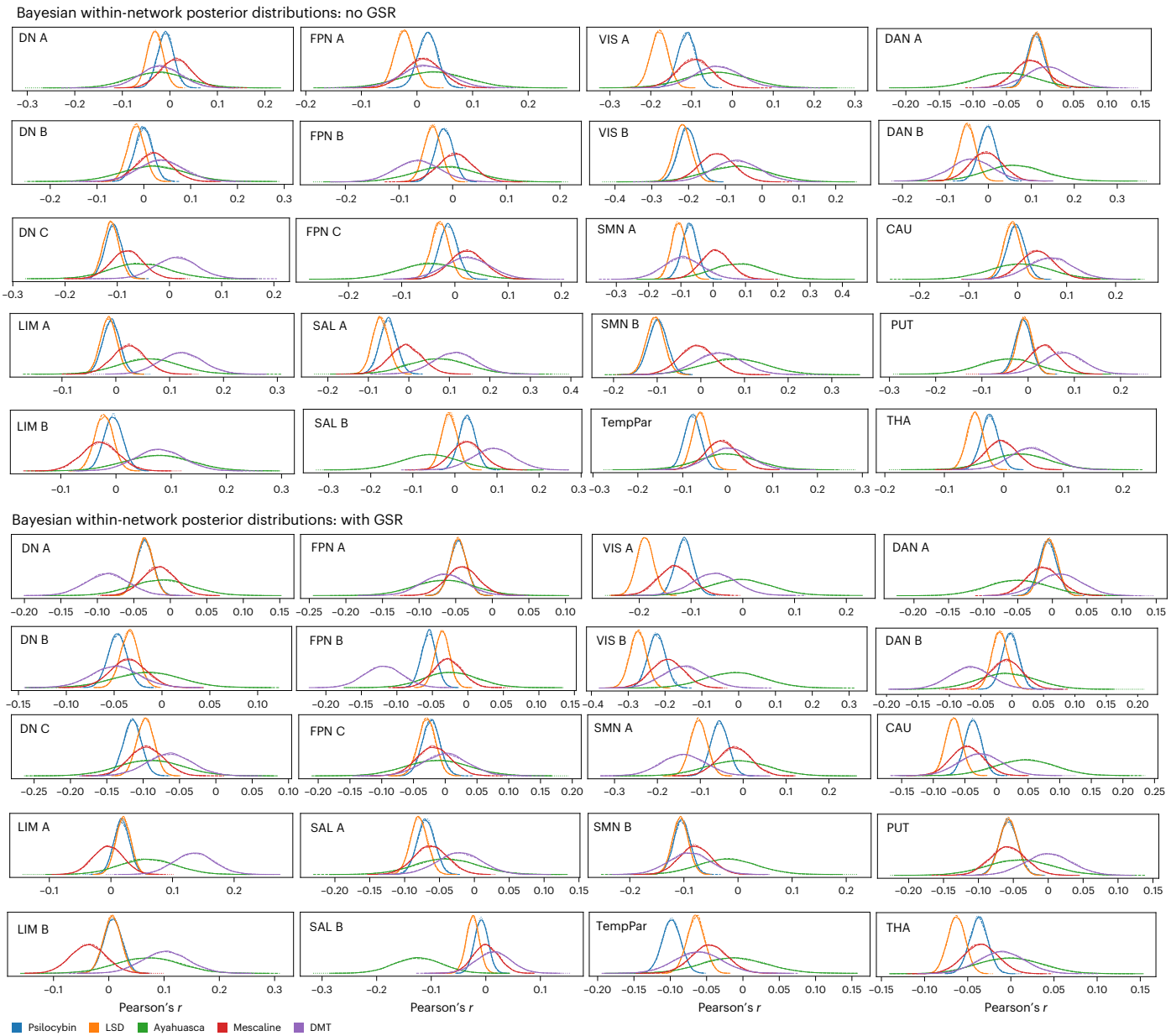

Fig. 4 | Bayesian posterior inference of within-network effects across drugs. Posterior distribution plots from the Bayesian hierarchical model showing the largest nonzero changes in within-network FC for each drug. These posterior distributions provide probabilistically grounded estimates of both the uncertainty (as indicated by distribution width) and magnitude (as indicated by the peak location on the *x* axis) of drug-induced effects for each modeled drug effect. The *x* axis represents the change in Pearson's correlation coefficient (*r*) between drug and placebo conditions, and the *y* axis reflects Bayesian probability density (arbitrary units). Each curve corresponds to a specific psychedelic.

directionality across several networks. Mescaline exhibited broadly similar but more variable effects, whereas DMT and ayahuasca showed wider, more dispersed posteriors, reflecting greater uncertainty, probably attributable to smaller sample sizes.

Without GSR, posterior distributions were shifted toward negative values across sensorimotor networks (VIS_A, VIS_B, SMN_A, SMN_B) and select hetero/transmodal networks (SAL_A, DN_C, TPar). On the whole, transmodal networks, including default and frontoparietal subnetworks, showed smaller and less consistent shifts, with posteriors frequently overlapping zero. With GSR, posterior distributions tended to be shifted further in the negative direction. However, this shift was nonuniform across drugs and networks, and several transmodal networks continued to exhibit substantial posterior overlap with zero. Subcortical regions, including the caudate, putamen and thalamus, also exhibited modest negative shifts in within-region coupling.

Discussion

There has been an upsurge of research activity on the neural underpinnings of the acute psychedelic experience in humans over the last decade. These efforts have produced a variety of relatively scattered findings, spanning several independent research groups across the globe. Owing to a variety of factors, this expanding literature is marked by heterogeneous and sometimes discrepant findings. Although much preclinical and wet laboratory science is challenging to homogenize and formally integrate, the brain imaging community has the key advantage of agreement on data formats, acquisition procedures and reference atlases.

This study represents the most comprehensive synthesis to date of how classic psychedelics modulate human brain circuit function. To reach this goal, we created an international consortium—the 'BOLD Psychedelic Consortium'—that aggregated and processed

Table 1 | Included psychedelic resting-state fMRI datasets

Original publication	Drug	Dosage/intake	Time since administration	Design	Total sample size (drug/placebo)	Country, University
Carhart-Harris et al., 2012[47]	Psilocybin	2 mg I.V.	Immediate	DB-RCT; within-subjects; counterbalanced	15 of 15 15 unique	UK, Imperial College London
Preller et al., 2020[22]	Psilocybin	0.2 mg kg^{-1} P.O.	70 mins post	DB-RCT; within-subjects; counterbalanced	23 of 23 23 unique	Switzerland, University of Zurich
Mason et al., 2020[15]	Psilocybin	0.17 mg kg^{-1} P.O.	102 mins post	DB-RCT; between-subjects; parallel group	26 of 24 50 unique	Netherlands, Maastricht University
Barrett et al., 2020[48]	Psilocybin	0.14 mg/kg^{-1} P.O.	90 mins post	DB-RCT; within-subjects; fixed order	19 of 19 19 unique	USA, Johns Hopkins University
Ley et al., 2023[49]	Psilocybin, LSD, mescaline	Psilocybin: 20 mg P.O. LSD: 100 µg P.O. Mescaline: 300 mg (n=16) 500 mg (n=16)	120 mins post	DB-RCT; within-subjects; counterbalanced	95 of 32 32 unique	Switzerland, University of Basel
Siegel et al., 2024[50]	Psilocybin	25 mg P.O.	60 mins post	DB-RCT; within-subjects; counterbalanced	11 of 11 11 unique	USA, Washington University St. Louis
Carhart-Harris et al., 2016[13]	LSD	75 µg I.V.	100 mins post	DB-RCT; within-subjects; counterbalanced	19 of 19 19 unique	UK, Imperial College London
Preller et al., 2018[23]	LSD	100 µg P.O.	75 mins post	DB-RCT; within-subjects; counterbalanced	25 of 25 25 unique	Switzerland, University of Zurich
Müller, et al., 2018[16]	LSD	100 µg P.O.	120 mins post	DB-RCT; within subjects; counterbalanced	50 of 50 50 unique	Switzerland, University of Basel
Palhano-Fontes et al., 2015[29]	DMT (Ayahuasca)	2.2 ml kg^{-1}, with 0.8 mg ml^{-1} of DMT and 0.21 mg ml^{-1} of harmine	40 mins post	Within-subjects; fixed order; no placebo	9 of 9 9 unique	Brazil, Federal University of Rio Grande do Norte
Timmermann et al., 2023[14]	DMT	20 mg I.V.	Immediate	DB-RCT; within subjects; counterbalanced	20 of 20 20 unique	UK, Imperial College London
					Total: 273 unique participants 560 connectomes	

I.V., intravenous; P.O., per os.

psychedelic-mediated changes uniformly in rsfMRI functional coupling profiles from 11 datasets spanning four psychedelic drugs, totaling 267 participants and over 500 connectomes. By implementing a fully Bayesian hierarchical modeling framework, we provide probabilistically grounded evidence for both shared and drug-specific alterations in FC within and between large-scale cortical networks and subcortical regions. Our findings reaffirm previous observations of psychedelic-induced enhanced whole-brain integration yet refine them by highlighting the changes in inter-network coupling links that exhibit the greatest robustness (defined here as high posterior confidence and low dispersion) across studies and by revealing effect specificity at the subnetwork and subcortical levels. We further note that, although certain patterns were apparent in mean FC matrices—such as reduced within-network coupling and increased THA-unimodal coupling—they did not always yield high-confidence posteriors. This reflects a core strength of the Bayesian approach: it considers jointly both the magnitude and uncertainty of an effect, discounting patterns with high between-subject variability or inconsistent replication across studies. In doing so, it avoids overinterpretation of apparent group-level trends and foregrounds the most robust and generalizable findings.

As our core conclusion, we found that psychedelics most robustly increase functional integration between select pairs of transmodal and unimodal subnetworks, as well as between key subcortical regions (PUT, CAU) and both unimodal and transmodal cortical areas. These conclusions are supported by posterior distributions showing high confidence (narrow dispersion) and consistent divergence from zero across compounds. In addition, our results challenge previous claims of widespread within-network disintegration[13,14,16,29], as Bayesian hierarchical modeling revealed limited and selective evidence for reductions in within-network FC, with few effects showing consistent divergence from zero. Instead, psychedelics seem to selectively reconfigure large-scale network–network interactions while modulating subcortical–cortical connectivity. Comparable analyses using ICA-AROMA-based denoising pipelines are reported in the Supplementary GitHub repository at https://github.com/banilo/BOLD_psychedelics_consortium. These showed broadly similar patterns of FC change, although with reduced effect magnitudes and notable sensitivity to the inclusion of GSR—highlighting the trade-offs between denoising stringency and preservation of neural signal. In sum, despite substantial methodological heterogeneity across studies, a core set of reproducible, cross-drug network changes emerged, pointing toward conserved neurobiological mechanisms across psychedelic drugs.

As the central finding of the present work, our analysis identified a brain signature of increased functional coupling between transmodal association circuits (FPN_A, FPN_B, FPN_C, DN_A, DN_B) and unimodal/heteromodal sensorimotor circuits (VIS_A, VIS_B, SMN_A, SMN_B, DAN_A, DAN_B). Notably, our Bayesian modeling revealed many high-confidence posterior probability distributions supporting these increases, particularly for LSD, psilocybin and mescaline, with some effects observed in amplified form for DMT. The stark reaction of transmodal systems under psychedelic effects is consistent with findings from high-resolution in vivo positron emission tomography imaging that have shown that the primary mechanistic target of psychedelics, the 5-HT2A receptor, is expressed most densely in transmodal (as well as VIS) cortices[30,31], and that these regions are among those showing statistically increased 5-HT2A occupancy after psilocybin administration[32,33]. Given that the unimodal–transmodal axis reflects a central cortical hierarchy separating sensorimotor from abstract cognitive processing[34,35], the

observed increase in their coupling suggests a flattening of this intrinsic processing hierarchy (cf. refs. 14,21). Although our FC data cannot determine directionality, these effects may arise from either increased top-down transmodal constraint or increased bottom-up influence from unimodal regions, both of which are plausible and supported by previous work. The former interpretation aligns with known patterns of task-dependent coupling between frontoparietal and sensory networks in goal-directed behavior[36,37]. The latter is consistent with evidence that 5-HT2A receptor activation disrupts transmodal cortical synchrony[13,38], potentially relaxing hierarchical precision weighting, as posited by the 'relaxed beliefs under psychedelics' model of psychedelic effects[39] and also consistent with the cortico-striato-thalamocortical gating model[1,40]. The pattern of increased unimodal–transmodal (and transmodal–transmodal) coupling under psychedelics, first shown by Roseman et al.[12], has been reported in several previous studies of LSD, psilocybin and DMT—all of which were included in the present analyses[9,12–18]. However, the precise spatial topography of this effect has varied across studies. Here we expanded upon these past studies and identified, with fine-grained subnetwork specificity and probabilistic likelihood, the specific unimodal and transmodal network pairs that exhibited the most reliable increases in connectivity across drugs and datasets. In particular, we found that regions within DN and FPN (sub)networks may show the most reliable increases in coupling with unimodal networks, reinforcing the notion that psychedelics may flatten lines of communication in the brain's intrinsic neural processing hierarchy.

Bayesian modeling also identified a robust pattern of intensified coupling between unimodal cortical networks and the dorsal striatum, particularly the CAU and PUT. Both the CAU and PUT receive dense convergent input from visual, motor and association cortices and play a central role in action selection, sensorimotor integration and the contextual modulation of perception and behavior[41,42]. Increased striatal coupling with unimodal cortex may therefore reflect altered weighting of corticostriatal interactions that link sensory input to motor and behavioral output, a process that is plausibly engaged during psychedelic states. These findings loosely align with cortico-striato-thalamocortical accounts of psychedelic action, which implicate changes in basal ganglia signaling in shaping large-scale information flow[1,40]. However, support for thalamic involvement was comparatively weaker in the present data. Although qualitative mean effects suggested increased coupling between thalamic regions (vTHA and dTHA) and unimodal cortex, these effects did not emerge as reliable in the Bayesian analyses. Instead, thalamocortical posteriors largely overlapped with zero, with a tendency toward weak negative shifts without GSR and moderately positive shifts with GSR. This pattern contrasts with previous reports emphasizing psychedelic-induced thalamic disinhibition and increased afferent flow to cortex[1,23,40,43,44], although important methodological differences—for example, analytic framework, parcellation strategy and treatment of global signal—limit direct comparability. Taken together, our findings indicate that striatal involvement represents the clearest and most reproducible subcortical feature of the observed connectivity changes.

Regarding within-network functional integration, our Bayesian findings point to a selective and modest set of effects, rather than widespread psychedelic-induced network 'disintegration' as has been reported previously (for example, refs. 13,14,27). Across networks, Bayesian posterior distributions revealed weak-to-moderate reductions in within-network FC, with substantial variability in effect magnitude and uncertainty across drugs, networks and preprocessing pipelines. Of note, many posterior distributions overlapped with zero, indicating that within-network effects were neither uniform nor universally robust. Within-network reductions were most consistent in sensorimotor (VIS and SMN) subnetworks, both with and without GSR. In contrast, hetero- and transmodal networks—including the DN, FPN, DAN and SAL—showed smaller and less reliable effects, with posterior mass frequently centered near zero. Notable exceptions include DN_C and SAL_A. Subcortical regions exhibited modest reductions in within-region coupling only after GSR. Broadly, the inclusion of GSR systematically shifted within-network estimates in a more negative direction; however, this effect was nonuniform across networks and drugs. An important point to note is that past work has applied primarily an ICA dual regression approach to assess within-network FC changes[12,13,29], whereas we applied an inter-regional FC approach. This may have influenced the observed effects (or lack thereof). Nonetheless, our finding of limited and heterogenous within-network effects with our analysis approach and Bayesian framework suggests that past work may have overestimated the robustness of this effect. Finally, our results also underscore the importance of fine-grained subnetwork analyses, which here revealed meaningful dissociations within networks that were obscured previously.

Although a core cross-drug signature was evident, our Bayesian modeling also revealed distinct connectivity profiles across individual psychedelics. We focus here on drug-induced effects that were broadly consistent across GSR and no GSR pipelines. LSD and psilocybin—our largest sample-size datasets—displayed virtually identical network-level alterations, consistent with their comparable pharmacological properties and phenomenological profiles[45,46]. Mescaline in turn exhibited a broadly similar pattern but with more selective enhancements in transmodal–unimodal integration and subcortical–cortical integration. DMT qualitatively exhibited the strongest network perturbations across all drugs. This trend was reflected in our Bayesian posterior distributions, though to a somewhat lesser extent than expected from raw effect size comparisons, probably due to high interindividual variability and the small sample size of the DMT dataset ($n = 15$). Ayahuasca, which contains DMT but also monoamine oxidase inhibitors, exhibited the most idiosyncratic connectivity profile, probably due to both its pharmacological complexity and its extremely small dataset ($n = 9$), which limits interpretability. Overall, although our study provides the most comprehensive evaluation to date of common psychedelic-induced connectivity changes, it remains challenging to draw strong conclusions regarding drug-specific effects. A complex mix of methodological and pharmacological factors probably contribute to the observed differences across drugs, including dosage, route of administration, receptor binding affinities (for example, 5-HT2A, 5-HT1A and others), time since drug administration and motion-related artefacts. Future studies should aim to directly compare different psychedelics under matched experimental conditions with standardized administration protocols and larger sample sizes to more precisely delineate the unique versus shared neural signatures of each compound (cf. ref. 30).

Despite the advantages of pooling data across several psychedelic neuroimaging studies, our mega-analytic approach carries important limitations. First, the included datasets varied in several fMRI acquisition parameters. Most notably, scanner field strength included 1.5 T (ayahuasca), 7 T (Maastricht psilocybin) and 3 T (all remaining datasets). Voxel size and repetition time also varied across studies (2–3 mm isotropic voxels; 2–3 s repetition time). Although our uniform preprocessing pipeline was designed to mitigate these differences, such variability inevitably introduces noise that may obscure more subtle effects. Second, although pooling subjects across several studies enhances confidence in the generalizability and robustness of findings, it does not guarantee data quality. Site-specific artifacts, residual physiological noise and unmeasured confounds may still propagate through the analysis, even with harmonized preprocessing and denoising. Head motion, in particular, remains a well-known concern in resting-state fMRI and is especially relevant here, given that participants tend to move more under the influence of psychedelics. To address this, we computed correlations between individual-level changes in framewise displacement (FD) and corresponding changes in FC. As shown in the Supplementary Information, these correlations

were weak-to-moderate, varied across drugs and did not resemble the spatial pattern of the observed drug effects. This suggests that our main findings are unlikely to be driven solely or systematically by motion-related artifacts. Third, as detailed in Table 1, studies varied in dosage, route of administration and latency of scanning relative to administration—all of which may also influence the observed effects. Although our Bayesian hierarchical modeling approach helps mitigate the impact of such heterogeneity, some residual influence is likely to persist. Finally, although our mega-analytic design was aimed at a harmonized analysis across studies, variability in study design remains. Although most datasets employed counterbalanced within-subject double-blind, randomized, controlled trials (DB-RCT) designs, one study lacked a placebo control and another used a fixed-order design—both of which may introduce confounds related to novelty, time or expectancy. Furthermore, although double-blinding aims to reduce bias, the strong psychological effects of psychedelics make true blinding difficult to maintain. Nevertheless, we believe that such expectancy and unblinding effects are less likely to substantially influence resting-state BOLD signal compared to subjective or clinical outcomes. Still, we acknowledge that design heterogeneity may contribute to residual variance in our findings. As the field advances, future collaborative efforts would benefit from prospectively harmonized multisite studies with standardized study designs, acquisition protocols, dosing regimens and participant selection criteria.

Our confederated effort is an instrumental step in bringing together the fragmented landscape of psychedelic research, yielding a more integrated whole that will in turn provide more clarity on the path forward. By coalescing rsfMRI data from several research groups across North America, South America and Europe, we identified a core, cross-drug signature of enhanced connectivity between transmodal association and unimodal sensorimotor networks, alongside enhanced selectively enhanced subcortical–cortical coupling and reduced subcortical–subcortical integration. These findings support neurocognitive models of psychedelic-induced hierarchical relaxation, while adding nuances to previous work by revealing fine-grained subnetwork and subcortex-specific effects. Contrary to some past findings, our mega-analytic approach did not find consistent evidence for within-network disintegration in the psychedelic state. Ultimately, cutting across methodological heterogeneity and additional limitations, our analysis revealed a robust cross-drug neural fingerprint of psychedelic states. As psychedelic research enters a new era of clinical and neuroscientific exploration, our findings provide a critical foundation upon which future investigations can build, ensuring that the field progresses toward greater rigor, reliability and translational impact.

Online content

Any methods, additional references, Nature Portfolio reporting summaries, source data, extended data, supplementary information, acknowledgements, peer review information; details of author contributions and competing interests; and statements of data and code availability are available at https://doi.org/10.1038/s41591-026-04287-9.

References

1. Vollenweider, F. X. & Preller, K. H. Psychedelic drugs: neurobiology and potential for treatment of psychiatric disorders. *Nat. Rev. Neurosci.* **21**, 611–624 (2020).
2. Rucker, J. J., Iliff, J. & Nutt, D. J. Psychiatry & the psychedelic drugs. Past, present & future. *Neuropharmacology* **142**, 200–218 (2018).
3. Nutt, D., Erritzoe, D. & Carhart-Harris, R. Psychedelic psychiatry's brave new world. *Cell* **181**, 24–28 (2020).
4. Andersen, K. A., Carhart-Harris, R., Nutt, D. J. & Erritzoe, D. Therapeutic effects of classic serotonergic psychedelics: a systematic review of modern-era clinical studies. *Acta Psychiatr. Scand.* **143**, 101–118 (2021).
5. Johnson, M. W., Hendricks, P. S., Barrett, F. S. & Griffiths, R. R. Classic psychedelics: an integrative review of epidemiology, therapeutics, mystical experience, and brain network function. *Pharmacol. Ther.* **197**, 83–102 (2019).
6. Kwan, A. C., Olson, D. E., Preller, K. H. & Roth, B. L. The neural basis of psychedelic action. *Nat. Neurosci.* **25**, 1407–1419 (2022).
7. Jaster, A. M. & González-Maeso, J. Mechanisms and molecular targets surrounding the potential therapeutic effects of psychedelics. *Mol. Psychiatry* **28**, 3595–3612 (2023).
8. McCulloch, D. E. W. Psychedelic resting-state neuroimaging: a review and perspective on balancing replication and novel analyses. *Neurosci. Biobehav. Rev.* **138**, 104689 (2022).
9. Girn, M. et al. A complex systems perspective on psychedelic brain action. *Trends Cogn. Sci.* **27**, 433–445 (2023).
10. Linguiti, S. et al. Functional imaging studies of acute administration of classic psychedelics, ketamine, and MDMA: methodological limitations and convergent results. *Neurosci. Biobehav. Rev.* **154**, 105421 (2023).
11. Moujaes, F. et al. Towards mapping neuro-behavioral heterogeneity of psychedelic neurobiology in humans. *Biol. Psychiatry* **93**, 1061–1070 (2023).
12. Roseman, L., Leech, R., Feilding, A., Nutt, D. J. & Carhart-Harris, R. L. The effects of psilocybin and MDMA on between-network resting state functional connectivity in healthy volunteers. *Front. Human Neurosci.* **8**, 204 (2014).
13. Carhart-Harris, R. L. et al. Neural correlates of the LSD experience revealed by multimodal neuroimaging. *Proc. Natl Acad. Sci. USA* **113**, 4853–4858 (2016).
14. Timmermann, C. et al. Human brain effects of DMT assessed via EEG-fMRI. *Proc. Natl Acad. Sci. USA* **120**, e2218949120 (2023).
15. Mason, N. et al. Me, myself, bye: regional alterations in glutamate and the experience of ego dissolution with psilocybin. *Neuropsychopharmacology* **45**, 2003–2011 (2020).
16. Müller, F., Dolder, P. C., Schmidt, A., Liechti, M. E. & Borgwardt, S. Altered network hub connectivity after acute LSD administration. *NeuroImage Clin.* **18**, 694–701 (2018).
17. Stoliker, D. et al. Neural mechanisms of resting-state networks and the amygdala underlying the cognitive and emotional effects of psilocybin. *Biol. Psychiatry* **96**, 57–66 (2024).
18. Madsen, M. K. et al. Psilocybin-induced changes in brain network integrity and segregation correlate with plasma psilocin level and psychedelic experience. *Eur. Neuropsychopharmacol.* **50**, 121–132 (2021).
19. Müller, F., Liechti, M. E., Lang, U. E. & Borgwardt, S. Advances and challenges in neuroimaging studies on the effects of serotonergic hallucinogens: contributions of the resting brain. *Prog. Brain Res.* **242**, 159–177 (2018).
20. Tagliazucchi, E. et al. Increased global functional connectivity correlates with LSD-induced ego dissolution. *Curr. Biol.* **26**, 1043–1050 (2016).
21. Girn, M. et al. Serotonergic psychedelic drugs LSD and psilocybin reduce the hierarchical differentiation of unimodal and transmodal cortex. *Neuroimage* **256**, 119220 (2022).
22. Preller, K. H. et al. Psilocybin induces time-dependent changes in global functional connectivity: Psi-induced changes in brain connectivity. *Biol. Psychiatry* **88**, 197–207 (2020).
23. Preller, K. H. et al. Changes in global and thalamic brain connectivity in LSD-induced altered states of consciousness are attributable to the 5-HT2A receptor. *Elife* **7**, e35082 (2018).
24. Li, X. et al. Moving beyond processing-and analysis-related variation in resting-state functional brain imaging. *Nat. Human Behav.* **8**, 2003–2017 (2024).
25. Researcher degrees of freedom. *Wikipedia* https://en.wikipedia.org/w/index.php?title=Researcher_degrees_of_freedom&oldid=1292410300 (2025).

26. Wicherts, J. M. et al. Degrees of freedom in planning, running, analyzing, and reporting psychological studies: a checklist to avoid p-hacking. *Front. Psychol.* **7**, 1832 (2016).
27. Bzdok, D., Floris, D. L. & Marquand, A. F. Analysing brain networks in population neuroscience: a case for the Bayesian philosophy. *Philos. Trans. R Soc. B* **375**, 20190661 (2020).
28. Kiesow, H. et al. 10,000 social brains: sex differentiation in human brain anatomy. *Sci. Adv.* **6**, eaaz1170 (2020).
29. Palhano-Fontes, F. et al. The psychedelic state induced by ayahuasca modulates the activity and connectivity of the default mode network. *PLoS ONE* **10**, e0118143 (2015).
30. Beliveau, V. et al. A high-resolution in vivo atlas of the human brain's serotonin system. *J. Neurosci.* **37**, 120–128 (2017).
31. Luppi, A. I. et al. A role for the serotonin 2A receptor in the expansion and functioning of human transmodal cortex. *Brain* **147**, 56–80 (2024).
32. Madsen, M. K. et al. Psychedelic effects of psilocybin correlate with serotonin 2A receptor occupancy and plasma psilocin levels. *Neuropsychopharmacology* **44**, 1328–1334 (2019).
33. Barrett, F. S. et al. Human cortical serotonin 2A receptor occupancy by psilocybin measured using [11C] MDL 100,907 dynamic PET and a resting-state fMRI-based brain parcellation. *Front. Neuroergon.* **2**, 784576 (2022).
34. Mesulam, M. From sensation to cognition. *Brain* **121**, 1013–1052 (1998).
35. Margulies, D. S. et al. Situating the default-mode network along a principal gradient of macroscale cortical organization. *Proc. Natl Acad. Sci. USA* **113**, 12574–12579 (2016).
36. Cole, M. W. et al. Multi-task connectivity reveals flexible hubs for adaptive task control. *Nat. Neurosci.* **16**, 1348 (2013).
37. Yeo, B. T. et al. Functional specialization and flexibility in human association cortex. *Cereb. Cortex* **25**, 3654–3672 (2015).
38. Muthukumaraswamy, S. D. et al. Broadband cortical desynchronization underlies the human psychedelic state. *J. Neurosci.* **33**, 15171–15183 (2013).
39. Carhart-Harris, R. L. & Friston, K. J. REBUS and the anarchic brain: toward a unified model of the brain action of psychedelics. *Pharmacol. Rev.* **71**, 316–344 (2019).
40. Doss, M. K. et al. Models of psychedelic drug action: modulation of cortical-subcortical circuits. *Brain* **145**, 441–456 (2022).
41. Haber, S. N. Corticostriatal circuitry. *Dialogues Clin. Neurosci.* **18**, 7–21 (2016).
42. Peak, J., Hart, G. & Balleine, B. W. From learning to action: the integration of dorsal striatal input and output pathways in instrumental conditioning. *Eur. J. Neurosci.* **49**, 658–671 (2019).
43. Preller, K. H. et al. Effective connectivity changes in LSD-induced altered states of consciousness in humans. *Proc. Natl Acad. Sci. USA* **116**, 2743–2748 (2019).
44. Avram, M. et al. Characterizing thalamocortical (Dys) connectivity following d-amphetamine, LSD, and MDMA administration. *Biol. Psychiatry Cogn. Neurosci. Neuroimaging* **7**, 885–894 (2022).
45. Holze, F. et al. Direct comparison of the acute effects of lysergic acid diethylamide and psilocybin in a double-blind placebo-controlled study in healthy subjects. *Neuropsychopharmacology* **47**, 1180–1187 (2022).
46. Nichols, D. E. Psychedelics. *Pharmacol. Rev.* **68**, 264–355 (2016).
47. Carhart-Harris, R. L. et al. Neural correlates of the psychedelic state as determined by fMRI studies with psilocybin. *Proc. Natl Acad. Sci. USA* **109**, 2138–2143 (2012).
48. Barrett, F. S., Doss, M. K., Sepeda, N. D., Pekar, J. J. & Griffiths, R. R. Emotions and brain function are altered up to one month after a single high dose of psilocybin. *Sci. Rep.* **10**, 2214 (2020).
49. Ley, L. et al. Comparative acute effects of mescaline, lysergic acid diethylamide, and psilocybin in a randomized, double-blind, placebo-controlled cross-over study in healthy participants. *Neuropsychopharmacology* **48**, 1659–1667 (2023).
50. Siegel, J. S. et al. Psilocybin desynchronizes the human brain. *Nature* **632**, 131–138 (2024).
51. Tian, Y., Margulies, D. S., Breakspear, M. & Zalesky, A. Topographic organization of the human subcortex unveiled with functional connectivity gradients. *Nat. Neurosci.* **23**, 1421–1432 (2020).
52. Buckner, R. L., Krienen, F. M., Castellanos, A., Diaz, J. C. & Yeo, B. T. The organization of the human cerebellum estimated by intrinsic functional connectivity. *J. Neurophysiol.* **106**, 2322–2345 (2011).
53. Schaefer, A. et al. Local-global parcellation of the human cerebral cortex from intrinsic functional connectivity MRI. *Cereb. Cortex* **28**, 3095–3114 (2018).

Manesh Girn[1] ✉, Manoj K. Doss[2], Leor Roseman[3], Katrin H. Preller[4], Fernanda Palhano-Fontes[5], Lorenzo Pasquini[1], Frederick S. Barrett[6], Pablo Mallaroni[7], Natasha L. Mason[7], Christopher Timmermann[3], Drummond E. McCulloch[8], Patrick M. Fisher[8], Brian S. Winston[6], Flora Moujaes[4], Felix Muller[9], Matthias E. Liechti[9], Franz X. Vollenweider[4], Johannes G. Ramaekers[7], Kim Kuypers[7], Draulio B. Araujo[5], Olaf Sporns[10], Joshua Siegel[11], Nico Dosenbach[11], David J. Nutt[3], Robin L. Carhart-Harris[1], Emmanuel A. Stamatakis[12] & Danilo Bzdok[13,14] ✉

[1]Department of Neurology, University of California San Francisco, San Francisco, CA, USA. [2]Department of Psychiatry and Behavioral Sciences, Center for Psychedelic Research and Therapy, The University of Texas at Austin Dell Medical School, Austin, TX, USA. [3]Department of Psychology, University of Exeter, Exeter, UK. [4]Department of Adult Psychiatry and Psychotherapy, University of Zurich, Zurich, Switzerland. [5]Brain Institute, Universidade Federal do Rio Grande do Norte, Natal, Brazil. [6]Center for Psychedelic and Consciousness Research, Johns Hopkins University School of Medicine, Baltimore,

MD, USA. [7]Department of Neuropsychology and Psychopharmacology, Faculty of Psychology and Neuroscience, Maastricht University, Maastricht, the Netherlands. [8]Neurobiology Research Unit, Rigshospitalet, Copenhagen, Denmark. [9]Department of Clinical Research, Clinical Pharmacology, University Hospital Basel, University of Basel, Basel, Switzerland. [10]Department of Psychological and Brain Sciences, Indiana University, Bloomington, IN, USA. [11]Department of Psychiatry, NYU Langone Center for Psychedelic Medicine, NYU Grossman School of Medicine, New York, NY, USA. [12]Division of Anaesthesia and Department of Clinical Neurosciences, University of Cambridge, Cambridge, UK. [13]Department of Biomedical Engineering, The Neuro - Montreal Neurological Institute (MNI), McConnell Brain Imaging Centre (BIC), McGill University, Montreal, Quebec, Canada. [14]Mila - Quebec Artificial Intelligence Institute, Montreal, Quebec, Canada. ✉e-mail: manesh.girn@ucsf.edu; danilo.bzdok@mcgill.ca

Methods

Data sources

This mega-analysis was designed and carried out as a community-wide effort that sought to integrate all available rsfMRI datasets examining the acute effects of classic serotonergic psychedelics in healthy adults. Eleven independently acquired fMRI neuroimaging datasets were ultimately included (Table 1). Access to these datasets was obtained by contacting the first and senior authors of the primary publications for previous acute psychedelic neuroimaging studies.

Our two core inclusion criteria were: (1) rsfMRI acquired during the acute effects of a classic psychedelic and (2) a healthy adult participant sample. To our knowledge, no eligible datasets were excluded for reasons other than feasibility of data sharing. One site—Copenhagen University Hospital (principal investigator P. Fisher)—was unable to contribute due to restrictions related to general data protection regulation. As of our final outreach in August 2024, we were not aware of any additional eligible datasets that were excluded due to lack of contact or nonresponse.

Of the 13 datasets, 12 were DB-RCTs that included a matched placebo condition. Most employed within-subject crossover designs with counterbalanced order of drug and placebo administration. One dataset[29] used a fixed-order design without a placebo condition. Table 1 summarizes the dosage, timing, and study design of each dataset. Full details on each dataset can be found in the original publications.

Brain signal preprocessing

All resting-state fMRI data underwent an identical preprocessing protocol using the fMRIprep software v.22.1.1[54]. This standardized, uniform preprocessing protocol was centrally coordinated and executed locally in an automated fashion in each laboratory where the data originated.

For each of the BOLD runs found per subject, our analytical protocol performed the following preprocessing steps. First, a reference volume and its skull-stripped version were generated using a custom methodology of fMRIPrep. The BOLD reference was then coregistered to the T1w reference using bbregister (FreeSurfer[55]), which implements boundary-based registration. Coregistration was configured with six degrees of freedom. Head motion parameters with respect to the BOLD reference (transformation matrices, and six corresponding rotation and translation parameters) were estimated before any spatiotemporal filtering using McFlirt (FSL[56]). BOLD runs were slice-time corrected using '3dTshift' from AFNI[57]. The BOLD timeseries were resampled onto their original, native space by applying the transforms to correct for head motion. We then resampled the ensuing voxelwise BOLD timeseries from individual subject space into standard anatomical reference space, generating preprocessed BOLD runs in the Montreal Neurological Institute (MNI) 152NLin2009cAsym 2-mm space. fMRIPrep then calculated the following confounds automatically based on the preprocessed BOLD: FD, spatial root mean square of the data after temporal differencing (DVARS)[58] and the global signal (mean signal within a whole-brain gray matter (GM) mask). FD and DVARS were calculated for each functional run, both using their implementations in Nipype.

All fMRIPrep outputs were generated by each site following fMRIPrep's standardized quality control protocols. This included verification of: (1) accurate brain extraction; (2) correct tissue segmentation into GM, white matter (WM) and cerebrospinal fluid (CSF); (3) precise coregistration between functional and anatomical images, with alignment confirmed in several planes; (4) appropriate normalization to MNI-space and (5) complete and accurate brain masking. Corresponding checks were guided by fMRIPrep-generated HTML reports and aligned with best practices from the Human Connectome Project. Each site conducted these checks before sharing preprocessed data with the central analysis team. Subjects showing poor registration, segmentation errors or mask artifacts were excluded.

To automatically remove high-motion subjects based on the obtained fMRIPrep QC outputs, we followed past work and excluded subjects which featured >15% of timepoints with FD > 0.5 (refs. 13,14,47,58). A total of six subjects were fully excluded from this study (five psilocybin, one DMT), corresponding to 12 total connectomes. An additional 29 connectomes were removed due to excessive motion at the session level (13 psilocybin, 7 LSD, 1 mescaline, 1 DMT and 7 placebo). Thus, a total of 41 connectomes were removed, resulting in a total of 519 remaining for the analyses.

Brain signal denoising

Following preprocessing, we applied four distinct pipelines to remove physiological, scanner-related and motion-related artifacts from the neuroimaging data, yielding four different sets of denoised brain signal volumes and, therefore, four sets of results. These pipelines included: (1 and 2) the anatomical CompCor (aCompCor) approach of Behzadi et al.[59], with and without GSR, and (3 and 4) the 'aggressive' ICA-AROMA approach of Pruim et al.[60], also with and without GSR. Pipelines 1 and 2 (aCompCor) are reported in the main text, whereas Pipelines 3 and 4 (ICA-AROMA) are included as a more stringent secondary approach in the Supplemental GitHub Repository at https://github.com/banilo/BOLD_psychedelics_consortium.

For the aCompCor-based pipelines, with and without GSR, a set of physiological regressors were extracted to allow for latent factor component-based noise correction[59]. Principal components were estimated after high-pass filtering the preprocessed BOLD timeseries using a discrete cosine filter (128-s cut-off). Probabilistic masks were generated in anatomical space for CSF and WM, and combined for an additional CSF + WM mask. Unlike the original implementation of aCompCor, which erodes the nuisance masks in BOLD space by contours of two voxels, we employed an anatomically informed refinement whereby a dilated GM mask, extracted from FreeSurfer's 'aseg' segmentation, was subtracted to avoid partial volume contamination[54]. This GM-removed CSF + WM mask was resampled into BOLD space and binarized at a 0.99 threshold. Components were extracted separately from each of CSF, WM and CSF–WM combined masks, with the top k components retained such that their timeseries cumulatively explained 50% of the variance within each mask. The remaining components were discarded from further analysis. These aCompCor-derived regressors were then used to denoise the BOLD signal with and without GSR.

In contrast, the ICA-AROMA-based pipelines, with and without GSR, involved applying ICA as a basis to classify and remove motion-related artifacts automatically. This was performed on MNI-space BOLD volumes that were first smoothed using a 6-mm FWHM Gaussian kernel (smoothing was applied only for ICA-based noise-versus-no-noise classification, not for final analysis). The fMRI timeseries data were decomposed into spatially independent components (ICs), which were then distinguished as signal or noise by a supervised pattern-learning algorithm using three features: (1) temporal correlation with motion parameters, (2) high-frequency spectral content and (3) spatial overlap with CSF or brain edges[60]. ICA-AROMA includes both 'nonaggressive' and 'aggressive' variants; we implemented the aggressive variant, which regresses only the noise ICs, thereby providing a more stringent denoising procedure compared to aCompCor. In contrast, the nonaggressive approach would have retained shared variance between signal and noise components, potentially leaving residual artifacts. By employing aggressive ICA-AROMA, we aimed to maximize noise removal; thus, using this approach as a conservative approach to compare with aCompCor. ICA-AROMA was applied with and without GSR.

Following denoising, all FC matrices were assessed using a standardized procedure. Each matrix was plotted using identical color scales and thresholds to ensure consistent evaluation across participants and studies. As part of our protocol, we checked and confirmed the presence of canonical resting-state network structure—specifically that within-network connectivity was visibly higher than between-network connectivity for key neural systems such as the default mode, VIS and SMN networks. Matrices were also assessed in terms of the direction and

relative magnitude of drug-induced changes and were confirmed to be consistent with those reported in the original studies for each dataset.

Regional and (sub)network parcellations

To facilitate comparability to other studies and aid neuroscientific interpretation, we extracted the denoised BOLD timeseries from cortical and subcortical regions using field-standard publicly available atlases. Cortical timeseries were extracted using the Schaefer et al.[53] local–global parcellation (100 region resolution and were grouped into large-scale subnetworks based on the 17 network assignments of Yeo et al.[61]). Subcortical timeseries were extracted using the Tian et al.[51] subcortical parcellation. The 'S2' parcellation was used for all nonthalamus subcortical regions (24 parcels total) and the 'S3' parcellation was used for the thalamus (14 parcels total), given the special interest in the latter in psychedelic research. CEREB timeseries were extracted using the Buckner et al.[52] cerebellar parcellation (17 parcels in total).

FC calculation

Interregional FC was calculated as the Pearson's product–moment correlation *r* between all parcels. Between-network FC corresponds to FC between parcels of different networks as defined based on the 17-network assignments of Yeo et al.[61], whereas within-network FC corresponds to FC between parcels of the same network.

As visualized in Fig. 1b,d below, we additionally computed parcel-wise measures that we refer to as 'within-network integration' and 'between-network integration', following Siegel et al.[50]. Defined here, 'within-network integration' corresponds to the mean FC of each parcel with all parcels within its Yeo–Schaefer network, whereas 'between-network integration' corresponds to the mean FC of each parcel with all parcels outside of its network. In this sense, it is a variant of previous global FC or 'global brain connectivity' approaches (for example, refs. 20,22).

Bayesian mega-analytic framework

We carried out a Bayesian mega-analysis to fully quantify the uncertainty of the different sources of variation at play, as a natural choice of method[62–64]. This step of our analysis workflow enabled the discovery and probabilistic characterization of the common neural features underlying psychedelic drug effects as captured by human brain imaging.

Motivations and advantages. Most previous neuroscience studies on psychedelic drugs attempted to draw sharp boundaries for regional drug effects using classical null hypothesis testing and *P* value thresholds. To overcome these limitations, the present work adopts Bayesian principles as a formal estimation framework to quantify the degree of change in functional coupling links under the psychedelic state. In contrast to frequentist post hoc estimations, the Bayesian regime provides a direct quantification of uncertainty around model parameters by appropriately handling all considered sources of variation. This enables more careful estimation of even very subtle drug effects. As an increasing trend, Bayesian mega-analysis has been used in medicine in high-stake areas such as to re-evaluate drug effects across several RCTs[65].

Bayesian hierarchical regression provides several key advantages relevant to the present aims: (1) it enables principled treatment of uncertainty by deriving full Bayesian posterior distributions for all measures, (2) it allows for continuous statements with explicitly quantified degrees of confidence (for example, 'How sure are we that these two drugs lead to similar changes in FC?') and (3) it does not require correction for multiple comparisons when models are independently specified, which is a key advantage as we can run one separate Bayesian model per brain feature[66]. More broadly, although frequentist models are designed to support binary decision-making under controlled assumptions (for example, rejecting a null hypothesis), Bayesian models are better suited for probabilistic reasoning about effect magnitudes and uncertainty. Rather than making dichotomous claims of presence or absence, our approach provides a graded, uncertainty-aware estimate of drug-related FC changes across diverse datasets. This distinction in modeling goals is especially relevant in the context of heterogeneous multisite neuroimaging data, where quantifying between-study variation is as important as identifying consistent effects.

Interpretation. Our analytical approach aimed to answer a distinct question: 'How certain are we that a particular psychedelic drug in a certain brain region leads to a drug-induced change in functional coupling, and how strong is this effect?' Accordingly, our models estimate the complete shape of the effect uncertainty of regional drug effects in the form of principled Bayesian posterior distributions. That is, our study did not ask 'Is there a strict categorical difference in inter-regional or inter-network FC between drug and placebo states?' Rather, we sought to directly quantify the population uncertainty distributions of functional coupling effects in relation to psychedelic drug influence, rather than focusing exclusively on mean FC differences. This modeling approach thus allows for probabilistic insight into the presence and strength of psychedelic effects across brain circuits, as well as their variability across drugs and studies. A fully specified generative model of the neural responses further opens the possibility to identify graded or overlapping shifts in brain network organization, consistent with the idea that drug-induced mental states may differ in degree rather than in kind[67].

Model specification. The random-effects probability model with parameters that vary by study and by drug, using a subject-wise MRI-derived brain measure as outcome and the experimental condition as input variable, had the following form:

Full Bayesian model specification.

Hyperpriors

$$\text{Hyper}_{\alpha} \sim \text{normal}\,(\mu = 0, \sigma = 1)$$

$$\text{Hyper}_{\beta} \sim \text{normal}\,(\mu = 0, \sigma = 1)$$

Priors

$$\alpha_{\text{study}\,j} \sim \text{normal}\,(\mu = \text{hyper}_{\alpha}, \sigma = 1)$$

$$\beta_{\text{drug}\_k} \sim \text{normal}\left(\mu = \text{hyper}_{\beta}, \sigma = 1\right)$$

Likelihood of linear model

$$y_{\text{conn\_link}} = \alpha\left[\text{studies}\right] + \beta_{\text{condition}}\left[\text{drugs}\right] \times \text{drug\_condition}$$

where α denotes the intercept parameter corresponding to each study j out of 11 total studies (datasets), bundled by the hyperprior hyper_{α}, β denotes the slope parameter explaining the presence of the psychedelic state in connectivity differences corresponding to drug k out of the 5 overall drugs, bundled by the across-drug hyperprior hyper_{β}, drug_condition denotes whether the observed resting-state scan was acquired during the placebo or drug-influenced state and $y_{\text{conn\_link}}$ captures a region-region functional coupling strength, initially computed by Pearson's correlation across the duration of a given resting-state brain scan in a particular participant, and then rescaled by Fisher *z* transformation (arctanh()) as outcome for this model estimation. As such, this model was inputted as many datapoints as we had resting-state scans (four-dimensional timeseries) from all 11 studies.

We approximated the model's joint posterior parameter distribution using Markov chain Monte Carlo sampling using the PyMC3 software. After 5,000 tuning steps, the sampler had converged to the stationary distribution. Subsequently, we drew 10,000 unbiased samples from the joint posterior distribution over all parameters in the model. We relied on performance metrics that are standards in Bayesian model estimation: (1) $\hat{R}$ to evaluate the quality of model fit for the model parameters and (2) effective sample size to index the efficiency of model convergence. A range of explanations for the brain–behavior relation between FC links and drug condition were browsed through by obtaining several plausible sets of model parameters, including their similarities and divergences, that could have generated the observed data.

For the purpose of validation of our modeling findings, we have computed three separate Markov chain Monte Carlo chains with different random initialization seeds but otherwise with the same data and same model specification. In other words, we have checked for the robustness of our model fit by rerunning the sampling process and testing whether it converges to the same final solution of posterior parameter distributions, that is, it reiterates the original modeling result.

Reporting summary

Further information on research design is available in the Nature Portfolio Reporting Summary linked to this article.

Data availability

Data access requests can be addressed to the respective study authors (Table 1).

Code availability

The full pipeline code in Python is openly available at https://github.com/banilo/BOLD_psychedelics_consortium.

References

54. Esteban, O. et al. fMRIPrep: a robust preprocessing pipeline for functional MRI. *Nat. Methods* **16**, 111–116 (2019).
55. Fischl, B. FreeSurfer. *Neuroimage* **62**, 774–781 (2012).
56. Jenkinson, M., Beckmann, C. F., Behrens, T. E., Woolrich, M. W. & Smith, S. M. FSL. *Neuroimage* **62**, 782–790 (2012).
57. Cox, R. W. AFNI: software for analysis and visualization of functional magnetic resonance neuroimages. *Comput. Biomed. Res.* **29**, 162–173 (1996).
58. Power, J. D., Barnes, K. A., Snyder, A. Z., Schlaggar, B. L. & Petersen, S. E. Spurious but systematic correlations in functional connectivity MRI networks arise from subject motion. *Neuroimage* **59**, 2142–2154 (2012).
59. Behzadi, Y., Restom, K., Liau, J. & Liu, T. T. A component based noise correction method (CompCor) for BOLD and perfusion based fMRI. *Neuroimage* **37**, 90–101 (2007).
60. Pruim, R. H. et al. ICA-AROMA: a robust ICA-based strategy for removing motion artifacts from fMRI data. *Neuroimage* **112**, 267–277 (2015).
61. Yeo, B. T. T. et al. The organization of the human cerebral cortex estimated by intrinsic functional connectivity. *J. Neurophysiol.* **106**, 1125–1165 (2011).
62. Smith, T. C., Spiegelhalter, D. J. & Thomas, A. Bayesian approaches to random-effects meta-analysis: a comparative study. *Stat. Med.* **14**, 2685–2699 (1995).
63. Bzdok, D. & Yeo, B. T. Inference in the age of big data: future perspectives on neuroscience. *Neuroimage* **155**, 549–564 (2017).
64. Biswal, B. B. et al. Toward discovery science of human brain function. *Proc. Natl Acad. Sci. USA* **107**, 4734–4739 (2010).
65. Spiegelhalter D. J., Abrams K. R. & Myles J. P. *Bayesian Approaches to Clinical Trials and Health-Care Evaluation* (Wiley, 2004).
66. Kruschke J. *Doing Bayesian Data Analysis: a Tutorial With R, JAGS, and Stan* 2nd edn (Academic, 2014).
67. Ritchie, S. J. et al. Sex differences in the adult human brain: evidence from 5216 UK biobank participants. *Cereb. Cortex* **28**, 2959–2975 (2018).

Acknowledgements

We thank R. McPhedrain for carefully reviewing and offering feedback on the analysis code and assisting with figure creation. D.B. was supported by the Brain Canada Foundation, through the Canada Brain Research Fund, with the financial support of Health Canada, National Institutes of Health (NIH R01 AG068563A, NIH R01 DA053301-01A1, NIH R01 MH129858-01A1), the Canadian Institute of Health Research (CIHR 438531, CIHR 470425), the Healthy Brains Healthy Lives initiative (Canada First Research Excellence fund), the IVADO R3AI initiative (Canada First Research Excellence fund) and by the CIFAR Artificial Intelligence Chairs program (Canada Institute for Advanced Research).

Author contributions

D.B., M.G. and E.A.S. initiated and led the BOLD Psychedelics consortium and the present study. All authors contributed to interpretation of the results and commenting on the manuscript draft.

Competing interests

M.G. is chief executive officer of Five Discovery, scientific advisor to the Center for MINDS, FIVE Research and Education, and is advisor and shareholder at EntheoTech Bioscience. D.B. is advisor and shareholder at Mindstate Design Labs and Biossil USA. F.S.B. is advisor and shareholder at Mindstate Design Labs, and is a scientific advisor for Wavepaths, Ltd and Lilly USA, LLC. M.K.D. is an advisor to VCENNA. L.P. is advisor and shareholder at AWEAR LLC. D.E.M.'s salary is supported by an unrestricted grant from COMPASS Pathways ltd. K.H.P. is an employee of Boehringer-Ingelheim GmBH & Co KG and serves as Chief Scientist of the Board of Directors of the Heffter Research Institute and is a scientific advisor to the Mind Foundation. R.L.C.-H. is a scientific advisor to TRYP therapeutics, Osmind, Mindstate Design Labs, Otsuka and Red Light Holland. The other authors declare no competing interests.

Additional information

Supplementary information The online version contains supplementary material available at https://doi.org/10.1038/s41591-026-04287-9.

Correspondence and requests for materials should be addressed to Manesh Girn or Danilo Bzdok.

Peer review information *Nature Medicine* thanks Michael Ferguson and the other, anonymous, reviewer(s) for their contribution to the peer review of this work. Primary Handling Editor: Jerome Staal, in collaboration with the *Nature Medicine* team.

nature portfolio

Corresponding author(s): Danilo Bzdok

Last updated by author(s): Sep 11, 2025

Reporting Summary

Nature Portfolio wishes to improve the reproducibility of the work that we publish. This form provides structure for consistency and transparency in reporting. For further information on Nature Portfolio policies, see our Editorial Policies and the Editorial Policy Checklist.

Statistics

For all statistical analyses, confirm that the following items are present in the figure legend, table legend, main text, or Methods section.

n/a	Confirmed
☐	☒ The exact sample size (*n*) for each experimental group/condition, given as a discrete number and unit of measurement
☐	☒ A statement on whether measurements were taken from distinct samples or whether the same sample was measured repeatedly
☒	☐ The statistical test(s) used AND whether they are one- or two-sided *Only common tests should be described solely by name; describe more complex techniques in the Methods section.*
☐	☒ A description of all covariates tested
☒	☐ A description of any assumptions or corrections, such as tests of normality and adjustment for multiple comparisons
☐	☒ A full description of the statistical parameters including central tendency (e.g. means) or other basic estimates (e.g. regression coefficient) AND variation (e.g. standard deviation) or associated estimates of uncertainty (e.g. confidence intervals)
☒	☐ For null hypothesis testing, the test statistic (e.g. *F*, *t*, *r*) with confidence intervals, effect sizes, degrees of freedom and *P* value noted *Give P values as exact values whenever suitable.*
☐	☒ For Bayesian analysis, information on the choice of priors and Markov chain Monte Carlo settings
☐	☒ For hierarchical and complex designs, identification of the appropriate level for tests and full reporting of outcomes
☐	☒ Estimates of effect sizes (e.g. Cohen's *d*, Pearson's *r*), indicating how they were calculated

Our web collection on statistics for biologists contains articles on many of the points above.

Software and code

Policy information about availability of computer code

Data collection	data collection was done prior to our study, as we perform a meta-analysis; please see Table 1 for detail how the eligible studies collected their data
Data analysis	several descriptive statistics in early Figure and then Bayesian meta-analysis as main analysis (Fig. 4 and 5)

For manuscripts utilizing custom algorithms or software that are central to the research but not yet described in published literature, software must be made available to editors and reviewers. We strongly encourage code deposition in a community repository (e.g. GitHub). See the Nature Portfolio guidelines for submitting code & software for further information.

Data

Policy information about availability of data

All manuscripts must include a data availability statement. This statement should provide the following information, where applicable:

- Accession codes, unique identifiers, or web links for publicly available datasets
- A description of any restrictions on data availability
- For clinical datasets or third party data, please ensure that the statement adheres to our policy

Data availability will be included

Research involving human participants, their data, or biological material

Policy information about studies with human participants or human data. See also policy information about sex, gender (identity/presentation), and sexual orientation and race, ethnicity and racism.

Reporting on sex and gender	Yes, as per previous studies included in present meta-analysis (Table 1).
Reporting on race, ethnicity, or other socially relevant groupings	n/a
Population characteristics	availabile in contributing studies
Recruitment	n/a
Ethics oversight	n/a

Note that full information on the approval of the study protocol must also be provided in the manuscript.

Field-specific reporting

Please select the one below that is the best fit for your research. If you are not sure, read the appropriate sections before making your selection.

☒ Life sciences ☐ Behavioural & social sciences ☐ Ecological, evolutionary & environmental sciences

For a reference copy of the document with all sections, see nature.com/documents/nr-reporting-summary-flat.pdf

Life sciences study design

All studies must disclose on these points even when the disclosure is negative.

Sample size	see Table 1
Data exclusions	This is a community wide effort; certain connectomes were excluded from further analysis based on excessive head motion during scanning.
Replication	Present meta-analysis attempts replication, each previous study already reported statistically significant results.
Randomization	explained in Table 1, for each study
Blinding	explained in Table 1, for each study

Reporting for specific materials, systems and methods

We require information from authors about some types of materials, experimental systems and methods used in many studies. Here, indicate whether each material, system or method listed is relevant to your study. If you are not sure if a list item applies to your research, read the appropriate section before selecting a response.

Materials & experimental systems

n/a	Involved in the study
☒	☐ Antibodies
☒	☐ Eukaryotic cell lines
☒	☐ Palaeontology and archaeology
☒	☐ Animals and other organisms
☒	☐ Clinical data
☒	☐ Dual use research of concern
☒	☐ Plants

Methods

n/a	Involved in the study
☒	☐ ChIP-seq
☒	☐ Flow cytometry
☐	☒ MRI-based neuroimaging

Plants

Seed stocks: n/a

Novel plant genotypes: n/a

Authentication: n/a

Magnetic resonance imaging

Experimental design

Design type: see previous studies (Table 1)

Design specifications: see previous studies (Table 1)

Behavioral performance measures: see previous studies (Table 1)

Acquisition

Imaging type(s): see previous studies (Table 1)

Field strength: see previous studies (Table 1)

Sequence & imaging parameters: see previous studies (Table 1)

Area of acquisition: see previous studies (Table 1)

Diffusion MRI ☐ Used ☒ Not used

Preprocessing

Preprocessing software: see previous studies (Table 1)

Normalization: see previous studies (Table 1)

Normalization template: see previous studies (Table 1)

Noise and artifact removal: see previous studies (Table 1)

Volume censoring: see previous studies (Table 1)

Statistical modeling & inference

Model type and settings: Bayesian hierarchical modeling

Effect(s) tested: functional connectivity incrase or decrease under psychedelic drug influence

Specify type of analysis: ☐ Whole brain ☒ ROI-based ☐ Both

Anatomical location(s): cortex, subcortex, cerebellum, thalamus

Statistic type for inference (See Eklund et al. 2016): Bayesian posterior parameter distributions

Correction: Bayesian joint parameter estimation

Models & analysis

n/a	Involved in the study
☐	☒ Functional and/or effective connectivity
☒	☐ Graph analysis
☒	☐ Multivariate modeling or predictive analysis

Functional and/or effective connectivity: Model inputs are estimates of functional connectivity strength